10.1098/rspa.2004.1315

THE ROYAL SOCIETY

Mechanisms of deep penetration of soft solids, with application to the injection and wounding of skin

By Oliver A. Shergold and Norman A. Fleck

Department of Engineering, University of Cambridge, Trumpington Street, Cambridge CB2 1PZ, UK (naf1@eng.cam.ac.uk)

Received 11 November 2003; accepted 2 March 2004; published online 13 July 2004

Micromechanical models are developed for the deep penetration of a soft solid by a flat-bottomed and by a sharp-tipped cylindrical punch. The soft solid is taken to represent mammalian skin and silicone rubbers, and is treated as an incompressible, hyperelastic, isotropic solid described by a one-term Ogden strain energy function. Penetration of the soft solid by a flat-bottomed punch is by the formation of a mode-II ring crack that propagates ahead of the penetrator tip. The sharp-tipped punch penetrates by the formation of a planar mode-I crack at the punch tip, followed by wedging open of the crack by the advancing punch.

For both modes of punch advance the steady-state penetration load is calculated by equating the work done in advancing the punch to the sum of the fracture work and the strain energy stored in the solid. For the case of a sharp penetrator, this calculation is performed by considering the opening of a plane-strain crack by a wedge using a finite-element approach. Analytical methods suffice for the flat-bottomed punch. In both models the crack dimensions are such that the load on the punch is minimized.

For both geometries of punch tip, the predicted penetration pressure increases with diminishing punch radius, and with increasing toughness and strain-hardening capacity of solid. The penetration pressure for a flat-bottomed punch is two to three times greater than that for a sharp-tipped punch (assuming that the mode-I and mode-II toughnesses are equal), in agreement with experimental observations reported in a companion paper.

Keywords: deep penetration; injection; fracture mechanics; finite-element method; soft solids

1. Introduction

The deep penetration of a soft solid by a punch is of widespread technological importance, with applications ranging from the piercing of mammalian skin by a hypodermic needle (or by a liquid jet) in administering an injection, to the failure of rubber seals or tyres by the penetration of a foreign body, such as a nail. The dependence of skin perforation upon the mechanical properties of skin, and the shape of the penetrator, is also relevant to the function and evolution of mammalian dentition: the successful predator must have sufficiently strong jaws and sharp teeth to cause skin perforation. And in remote robotic surgery, as well as in training simulators for surgical techniques, it is important to quantify the resistance of tissue to penetration.

 © 2004 The Royal Society

Table 1. *Summary of penetration experiments from the literature*

(SF, Shergold & Fleck (2004); V, Vijay (1989); Kn, Knight (1975); OC, O'Callaghan *et al.* (1999); FB, Figge & Barnet (1948); SK, Stephens & Kramer (1964); B, Brett *et al.* (1997); SM, Schramm & Mitragotri (2002); F, Frick *et al.* (2001); A, Ankerson *et al.* (1999); Bl, Black *et al.* (1985); KT, Katakura & Tsuji (1985); C, Charrier *et al.* (1986); SA, Stevenson & Abmalek (1994); L, Livingston *et al.* (1961).)

	type of penetrator					
class of soft solid	knife blade	needle	conical-tipped punch	ball-ended punch	flat-bottomed punch	high-speed liquid jet
human skin *in vivo*	—	SF	—	—	SF	V, SF
human cadaver skin	Kn, OC	FB, SK, B	—	—	—	SK, FB, SM
human cadaver fat and muscle	OC	FB, B	—	—	—	FB, SM
sheep skin *in vitro*	—	F	—	—	—	—
pig skin *in vitro*	A, Bl	B	—	—	—	SM
ox skin *in vitro*	—	—	—	—	—	KT
silicone rubber	—	—	SF	—	SF	—
natural rubber	—	—	C	SA, C	SA, L	—
styrene-butadiene rubber	—	—	—	—	L	—

Investigations into the puncture of human cadavers and animal skin with needles and knives highlight the sensitivity of the penetration force to the geometry of the penetrator, type of tissue, and loading parameters, such as the degree of pre-stretch of the skin and the velocity of the penetrator. Pertinent details of these investigations are reviewed below and summarized in table 1.

(*a*) *Mechanisms of penetration*

Despite the ubiquitous nature of soft solid penetration, the existing literature provides little insight into the underlying mechanisms of penetration. The medical literature on skin injection, and the mechanical engineering literature on rubber penetration, indicate that deep penetration involves cracking of the soft solid, followed by substantial reversible deformation when the penetrator is removed (Stephens & Kramer 1964; Katakura & Tsuji 1985; Stevenson & Abmalek 1994).

A limited number of experimental studies reveal that the crack geometry is sensitive to the punch-tip geometry and to the material properties of the penetrated

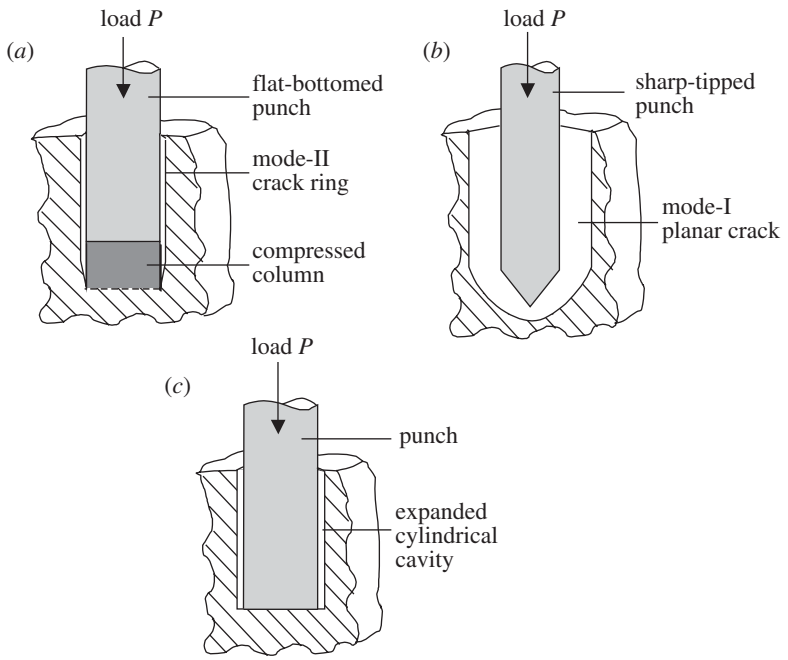

Figure 1. Penetration mechanisms of a soft solid by: (*a*) a flat-bottomed punch; (*b*) a sharp-tipped punch. (*c*) Penetration of a strong solid by a flat-bottomed or sharp-tipped punch.

solid. Stevenson & Abmalek (1994) showed that a flat-bottomed punch penetrates natural rubbers by the formation of a mode-II ring crack that propagates ahead of the penetrator tip, as shown in figure 1*a*. In a companion paper to the present study, Shergold & Fleck (2004) observed that a sharp-tipped punch penetrates silicone rubber and skin by the formation of a planar mode-I crack ahead of the tip; the crack faces are wedged open by the advancing punch, as shown in figure 1*b*. They also confirmed that a flat-bottomed punch penetrates silicone rubber and skin by the mode-II ring-crack mechanism of Stevenson & Abmalek (1994). The main purpose of the present paper is to develop quantitative models for the penetration of soft materials by flat-bottomed and sharp-tipped punches by the mechanisms shown in figure 1. These models are justified by drawing upon salient experimental results taken from the companion paper (Shergold & Fleck 2004).

The penetration mechanism observed for soft solids is different from that for strong, ductile solids such as metals, soils and polymers. Deep penetration of strong solids involves radial expansion of material at the penetrator tip (see figure 1*c*) (Bishop *et al*. 1945; Hill 1950; Gibson 1950; Gibson & Anderson 1961; Scott 1980; Wright *et al*. 1992). Bishop *et al*. (1945) modelled penetration by the expansion of a cavity in an elastic-ideally plastic solid, and argued that the penetration pressure is comparable with the cavitation pressure p_c, defined by the pressure to expand the cavity from zero initial radius to a finite final radius. They showed that the cavitation pressure for an expanding spherical cavity is close to that for a cylindrical cavity and so the precise details of the cavity shape are relatively unimportant in the prediction of the penetration pressure. Typically, for metals p_c is of the order of four to five times the uniaxial yield strength, depending upon the yield strain and the strain-hardening

rate. Wright *et al.* (1992) have applied this model to the case of deep penetration of polymers, and showed that the cavitation pressure p_c becomes infinite when the strain-hardening behaviour is strongly exponential in character. They found experimentally, and argued theoretically, that penetration involves a cracking mechanism in addition to hole expansion for polymers displaying exponential hardening. Wright *et al.* (1992) were able to make accurate predictions by including a 'hackle zone' within the cavity expansion model.

(*b*) *The measured penetration force for soft solids*

Several researchers (Figge & Barnet 1948; Livingston *et al.* 1961; Knight 1975; Black *et al.* 1985; Charrier *et al.* 1986; Towler *et al.* 1988; Brett *et al.* 1997; Ankerson *et al.* 1998, 1999; O'Callaghan *et al.* 1999; Frick *et al.* 2001) have studied the force required to penetrate mammalian skin and rubber, although none of these studies have led to quantitative models for the penetration of a soft solid. It is well established that the penetration force decreases with increasing sharpness of penetrator (see, for example, the experiments on cutting cadaver skin by Knight (1975)). The penetration force is also sensitive to the type of tissue being incised: O'Callaghan *et al.* (1999) demonstrated that the penetration force for skin and muscle is significantly higher than that for fat. Brett *et al.* (1997) have noted much higher penetration forces for pig skin than for human skin, whereas the penetration force through the underlying tissues is similar for pigs and humans.

Unfortunately, the dependencies of the penetration force upon the strength of the skin and upon the level of pre-stretch are not straightforward. Ankerson *et al.* (1999) observed that the peak penetration force for knife incision of pig skin is similar to that for synthetic chamois, despite a large difference in tensile strengths. Frick *et al.* (2001) preloaded strips of sheep skin (removed from the carcass) and reported that the force required to puncture the sample with a suture needle increased with increasing pre-tension in the skin. By contrast, Figge & Barnet (1948) performed tests on cadavers with a needle injector and demonstrated that less force is required to penetrate stretched skin than loose skin. This difference in behaviours may be attributed to the differences in constraint on the skin: when cadaver skin is loose, the needle injector compresses the skin against the underlying muscle fascia and the penetration load is high. Alternatively, when cadaver skin is pre-stretched and then subjected to a needle injector, the skin remains unsupported by the underlying muscle fascia, and the penetration force is low.

Contradictory evidence also exists for the relation between injector speed and force. Frick *et al.* (2001) found that the injector force did not change when the needle velocity was increased from 1 to 10 mm s^{-1}. However, Brett *et al.* (1997) found that the penetration force was speed dependent: a Tuohy needle was used in penetration studies on the ligamentum flavum (the membrane protecting the epidural cavity around the spinal cord), and it was found that the force decreased with increasing speed in the range 1–3 mm s^{-1}.

(*c*) *Liquid-jet injection of skin*

The conventional method of drug delivery by injection involves the slow insertion of a hollow hypodermic needle, with subsequent injection through the needle once the skin has been perforated. An alternative method of injection is to deliver the

drug as a high-pressure liquid jet with a diameter within the range 0.1–0.5 mm, with sufficient intensity to pierce the skin. Clinical studies investigating the *in vivo* performance of liquid-jet injectors indicate that the success of injecting the full dose of drug is dependent upon both the skin type and the site of injection on the body (Verhagen *et al*. 1995; Cooper *et al*. 2000). A review of accidents involving high-pressure liquid jets (Vijay 1989) and a review of needle-free injector designs (Maas & Brink 1987) each detail the combinations of liquid pressures and jet diameters that have penetrated the skin. These data are useful for indicating the *sufficient* condition for penetration, but give no insight into the threshold injection pressure for skin penetration: that is the *necessary* and *sufficient* condition. In broad terms, these data suggest that a pressure of 15 MPa is adequate for the perforation of human skin by a jet of diameter in the range 0.1–0.5 mm.

(*d*) *Outline of the paper*

The structure of the current study is as follows. First, a constitutive description is given for the stress-versus-strain response of rubber-like materials with a wide range of strain-hardening behaviours. This constitutive description is used in both the flat-bottomed punch and sharp-tipped punch penetration models. Then, penetration models are presented for the penetration of an incompressible, hyperelastic, isotropic solid by a flat-bottomed punch and a sharp-tipped punch. For each model the crack geometry is obtained by minimizing the load for steady-state penetration with respect to the dimensions of the crack. The flat-bottomed punch problem is solved analytically, while a finite-element approach is required for the sharp-tipped punch penetration model. For each model the steady-state penetration load is calculated for a range of material responses (strain hardening and toughness) and punch diameters. Direct comparisons of the predictions are made with the measured penetration loads (and crack dimensions) taken from the companion experimental study (Shergold & Fleck 2004).

2. Rubber-like constitutive models

The constitutive description of the soft solid is taken to be the Ogden (1972) model for an incompressible, isotropic, hyperelastic solid. This model describes a wide range of strain-hardening behaviours and is readily available within finite-element codes such as Abaqus. Throughout this paper we use a modified form of the one-term Ogden strain-energy density function

$$\phi = \frac{2\mu}{\alpha^2}(\lambda_1^\alpha + \lambda_2^\alpha + \lambda_3^\alpha - 3), \tag{2.1}$$

where ϕ is the strain-energy density per undeformed unit volume, α is a strain-hardening exponent, μ is the shear modulus under infinitesimal straining and λ_i are the principal stretch ratios. This form of the Ogden strain-energy density is consistent with that used by the finite-element analysis software Abaqus version 6.3†.

The use of a strain-energy density function for proportional and near proportional straining is rigorous for both conservative materials, such as rubber, and for elastic-

† Hibbit, Karlsson and Sorensen, Inc., Pawtucket, RI, USA.

Table 2. *Curve fits of the Ogden constitutive law (2.1), and toughness values of solids used in penetration experiments reported by Shergold & Fleck (2004)*

solid	grade	μ (MPa)	α	J_{IC} (kJ m^{-2})
silicone rubber	Sil8800	2.7	2.5	3.1
silicone rubber	B452	0.40	3.0	3.8
human skin		0.11	9.0	2.5

plastic solids (see, for example, Fung 1981). The assumption that skin is incompressible has been justified by a number of investigators (Ankerson *et al*. 1999; Reihsner *et al*. 1995; North & Gibson 1978; Vossoughi & Vaishnav 1979).

Table 2 gives the values of the Ogden constants determined by Shergold & Fleck (2004) for two grades of silicone rubber (Sil8800 and B452) and human skin. It is shown in our companion study that the one-term Ogden model gives a reasonable approximation to the concave (J-shaped) stress-versus-strain curve observed for skin and silicone rubber. Shergold & Fleck (2004) used the tensile uniaxial stress-versus-strain response measured by Jansen & Rottier (1958) in order to determine the Ogden constants for human skin; Jansen & Rottier (1958) took skin samples 80 mm laterally from the median line between the umbilic and pubic area. Shergold & Fleck also performed tensile and compressive uniaxial stress-versus-strain tests on the silicone rubbers (Sil8800 and B452) in order to determine their respective Ogden constants.

Values for the toughness J_{IC} are included in table 2; the values for the silicone rubbers were determined using a trouser-tear test and are taken from Shergold & Fleck (2004), while the toughness value of human skin has been measured by Pereira *et al*. (1997) using a scissor tear test.

3. Flat-bottomed punch penetration model

We begin by summarizing the model of Stevenson & Abmalek (1994) for the penetration of a soft solid by a flat-bottomed circular cylindrical punch. The development given below makes use of the Ogden formulation of elastic strain energy, whereas Stevenson & Abmalek (1994) made use of the Mooney–Rivlin formulation. The stress–strain curves given in our companion study reveal a high-strain-hardening behaviour at large strains, which is adequately described by the Ogden description but not by the Mooney–Rivlin description.

Consider a frictionless, flat-bottomed, rigid cylindrical punch of radius R penetrating a semi-infinite block, as sketched in figure 2*a*. A ring crack propagates ahead of the penetrator tip forming a column, which in the undeformed configuration has a radius b and a length ℓ (see figure 2*b*). The punch shortens the column from an undeformed length ℓ to a compressed length $(\ell - h)$. Simultaneously, the radius of the column increases from b to R, due to incompressibility. The penetration load P_{F} is estimated by equating the work done in advancing the punch to the sum of the crack work and the strain energy S in the penetrated solid. There are two contributions to S: that due to compression of the column, S_{C}, and that due to expansion of the hole, S_{H}.

Consider steady-state penetration of the punch at a fixed load P_{F}. In the current state the punch has descended by a depth h. The work done by the punch upon

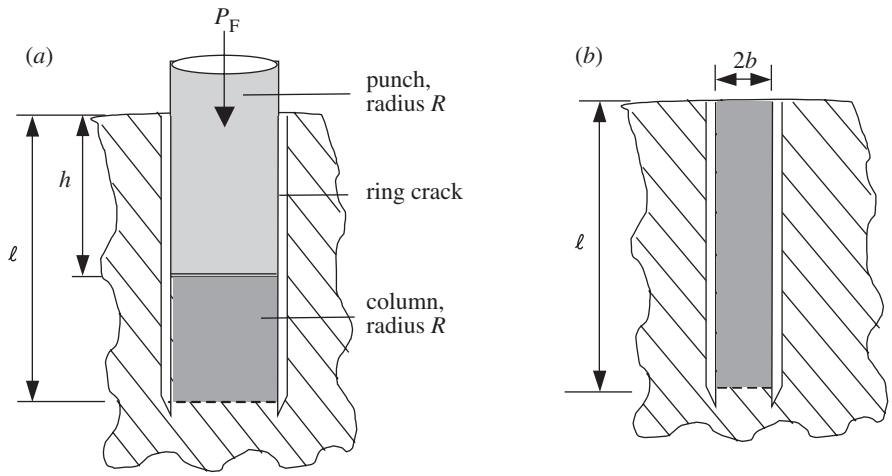

Figure 2. (*a*) Steady-state penetration of a soft solid by a flat punch and (*b*) stress-free configuration after punch removal.

advancing by an increment δh is given by

$$P_{\mathrm{F}}\delta h = 2\pi b J_{\mathrm{IIC}}\delta\ell + \frac{\partial S_{\mathrm{C}}}{\partial \ell}\delta\ell + \frac{\partial S_{\mathrm{H}}}{\partial \ell}\delta\ell, \tag{3.1}$$

where J_{IIC} is the toughness of the material to mode-II crack propagation. The quantity $\partial S_{\mathrm{C}}/\partial\ell$ is the work done per unit depth (in the undeformed configuration) in order to compress the column beneath the punch by an axial stretch factor of $\lambda_z = b^2/R^2$, upon noting incompressibility. $\partial S_{\mathrm{H}}/\partial\ell$ is the energy stored within unit thickness (undeformed) of the solid external to the hole. Explicit expressions for $\partial S_{\mathrm{C}}/\partial\ell$ and $\partial S_{\mathrm{H}}/\partial\ell$ are obtained below. It is convenient at this point to use dimensional analysis to write

$$\frac{1}{\pi\mu R^2}\left(\frac{\partial S_{\mathrm{C}}}{\partial \ell} + \frac{\partial S_{\mathrm{H}}}{\partial \ell}\right) = f\left(\frac{b}{R}\right), \tag{3.2}$$

where the non-dimensional function $f(b/R)$ remains to be determined.

Substitution of (3.2) into (3.1) defines the average penetration pressure p_{F} on the end of the punch as

$$\frac{p_{\mathrm{F}}}{\mu} = \frac{P_{\mathrm{F}}}{\pi\mu R^2} = \left[\frac{2b}{R}\frac{J_{\mathrm{IIC}}}{\mu R} + f\left(\frac{b}{R}\right)\right]\frac{\partial\ell}{\partial h}. \tag{3.3}$$

Since the solid is taken as incompressible, volume conservation of the column gives

$$\pi R^2(\ell - h) = \pi b^2 \ell, \tag{3.4}$$

and (3.3) can be rewritten as

$$\frac{p_{\mathrm{F}}}{\mu} = \left[1 - \left(\frac{b}{R}\right)^2\right]^{-1}\left[\frac{2b}{R}\frac{J_{\mathrm{IIC}}}{\mu R} + f\left(\frac{b}{R}\right)\right]. \tag{3.5}$$

(*a*) *Calculation of the stored strain energy*

We now obtain expressions for $\partial S_{\mathrm{C}}/\partial\ell$ and $\partial S_{\mathrm{H}}/\partial\ell$. First, consider the strain energy stored in the solid due to expansion of the hole.

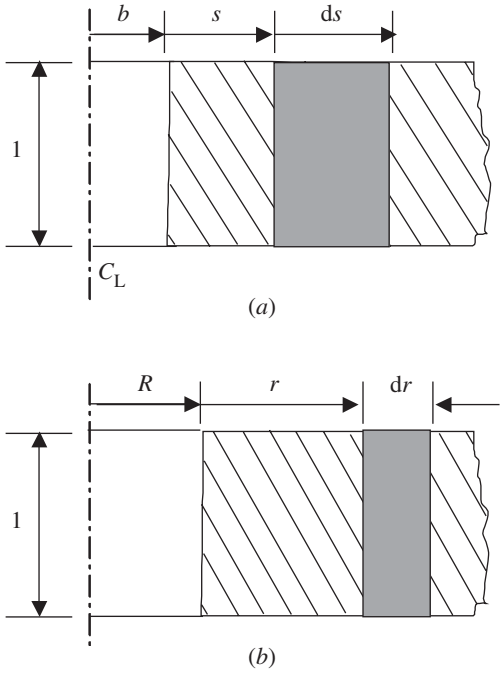

Figure 3. Expansion of a cylindrical annulus of the solid of unit height from a radius s to a radius r, on expansion of the hole from a radius b to a radius R: (a) undeformed configuration, (b) deformed configuration.

(i) *Strain energy stored due to hole expansion*

Stevenson & Abmalek (1994) follow the approach of Bishop *et al*. (1945) in determining $\partial S_{\mathrm{H}}/\partial \ell$. However, for materials where the stress-versus-strain response is defined by a strain energy function, we propose a simpler method to determine $\partial S_{\mathrm{H}}/\partial \ell$. Consider a representative cylindrical annulus of the solid in the undeformed configuration. The annulus has an initial radius s, thickness ds and unit height, see figure 3a, and expands to a radius r, thickness dr and unit height, as shown in figure 3b.

Volume conservation for the incompressible solid dictates that

$$r^2 - R^2 = s^2 - b^2 \tag{3.6}$$

and $\lambda_r \lambda_\theta \lambda_z = 1$, where λ_r, λ_θ and λ_z are the principal stretch ratios in a polar cylindrical coordinate system.

The assumption of plane-strain hole expansion implies $\lambda_z = 1$ and hence

$$\lambda_\theta = \frac{1}{\lambda_r} = \frac{r}{s}. \tag{3.7}$$

The Ogden expression (2.1) for the strain-energy density $\phi(s)$ of the annulus in the undeformed configuration is

$$\phi(s) = \frac{2\mu}{\alpha^2}\left[\left(\frac{r}{s}\right)^{\alpha} + \left(\frac{s}{r}\right)^{\alpha} - 2\right]. \tag{3.8}$$

Hence the stored strain energy within the solid, associated with hole expansion from a radius b to a radius R, is

$$\frac{\partial S_{\mathrm{H}}}{\partial \ell} = \int_b^\infty 2\pi s\phi(s)\,\mathrm{d}s = \int_R^\infty 2\pi r\phi\,\mathrm{d}r. \tag{3.9}$$

Now introduce the normalization,

$$\eta = \left(\frac{r}{R}\right)^2, \tag{3.10}$$

so that (3.8) and (3.9) give

$$\frac{\partial S_{\mathrm{H}}}{\partial \ell} = \pi R^2 \int_1^\infty \frac{2\mu}{\alpha^2} g\left(\eta, \frac{b}{R}\right) \mathrm{d}\eta, \tag{3.11}$$

where

$$g\left(\eta, \frac{b}{R}\right) = \left(1 - \frac{1-(b/R)^2}{\eta}\right)^{\alpha/2} + \left(1 - \frac{1-(b/R)^2}{\eta}\right)^{-\alpha/2} - 2. \tag{3.12}$$

In general, (3.12) must be integrated numerically, but for the choice $\alpha = 2$ it can be integrated analytically to read

$$\frac{\partial S_{\mathrm{H}}}{\partial \ell} = \pi\mu R^2 \left(\frac{b^2}{R^2} - 1\right) \ln\left(\frac{b}{R}\right). \tag{3.13}$$

(ii) *Stored strain energy due to compression of the column*

Now consider the strain energy $\partial S_{\mathrm{C}}/\partial \ell$ associated with compression of a column of unit undeformed length and radius b to a current radius of R. For a polar cylindrical coordinate system the principal stretch ratios for column compression are

$$\lambda_r = \lambda_\theta = \frac{1}{\sqrt{\lambda_z}} = \frac{R}{b}. \tag{3.14}$$

The one-term Ogden strain energy function is

$$\phi = \frac{2\mu}{\alpha^2}(2\lambda_r^\alpha + \lambda_r^{-2\alpha} - 3) \tag{3.15}$$

and the strain energy in the column $\partial S_{\mathrm{C}}/\partial \ell$ of radius b and unit depth is

$$\frac{\partial S_{\mathrm{C}}}{\partial \ell} = \pi R^2 \frac{2\mu}{\alpha^2}\left[2\left(\frac{b}{R}\right)^{2-\alpha} + \left(\frac{b}{R}\right)^{2\alpha+2} - 3\left(\frac{b}{R}\right)^2\right]. \tag{3.16}$$

(iii) *Non-dimensional stored-strain-energy function*

Recall from (3.2) that the sum

$$\frac{\partial S_{\mathrm{C}}}{\partial \ell} + \frac{\partial S_{\mathrm{H}}}{\partial \ell}$$

can be stated in terms of a non-dimensional function $f(b/R)$. The expressions (3.11) and (3.16) allow $f(b/R)$ to be stated explicitly as

$$f\left(\frac{b}{R}\right) = \frac{2}{\alpha^2}\left\{\left[2\left(\frac{b}{R}\right)^{2-\alpha} + \left(\frac{b}{R}\right)^{2\alpha+2} - 3\left(\frac{b}{R}\right)^2\right] + \int_1^\infty g\left(\eta, \frac{b}{R}\right)\mathrm{d}\eta\right\}, \tag{3.17}$$

where $g(\eta, (b/R))$ is given by (3.12).

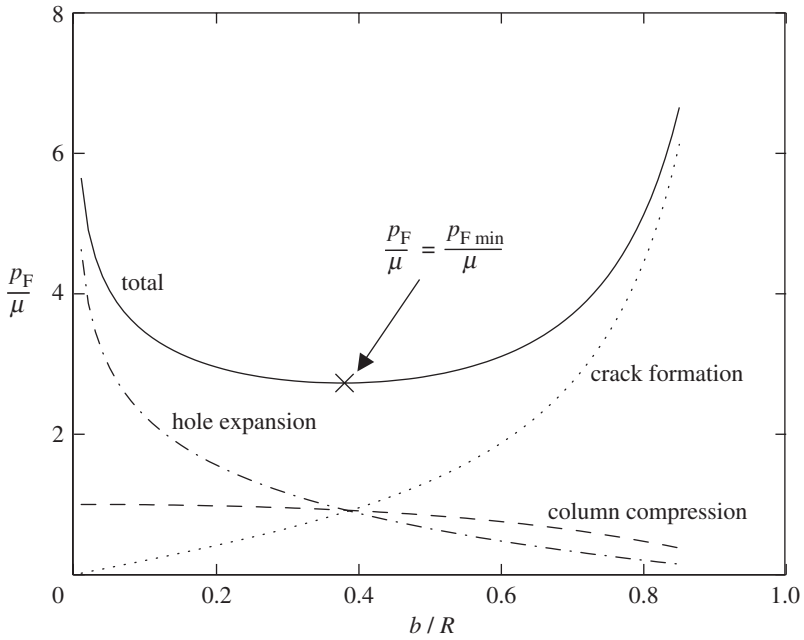

Figure 4. Penetration of a soft solid by a flat-bottomed punch for $\alpha = 2$ and $J_{IIC}/\mu R = 1$. Contributions to p_F/μ from crack formation, hole expansion and column compression are given as a function of b/R.

(*b*) *Prediction of the diameter of the cylindrical crack*

We note from (3.5) and (3.17) that the magnitude of p_F/μ comprises contributions from the mechanisms of crack formation, hole expansion and column compression. These separate contributions are plotted in figure 4 as a function of b/R for a solid with α taken to be 2 for simplicity. For low values of b/R the stored strain energy associated with hole expansion is the dominant contributor to p_F/μ, while at high values of b/R the work of crack formation is the dominant term. A global minimum $p_{F\,min}/\mu$ in p_F/μ exists at an intermediate value of b/R.

It is argued that stable penetration occurs at this minimum value of pressure. The relation (3.5) achieves a minimum value $p_{F\,min}/\mu$ when b/R satisfies the relation

$$\frac{J_{IIC}}{\mu R}\left[1+\left(\frac{b}{R}\right)^2\right] = -\frac{1}{2}\left[1-\left(\frac{b}{R}\right)^2\right] f'\left(\frac{b}{R}\right) - \left(\frac{b}{R}\right) f\left(\frac{b}{R}\right), \tag{3.18}$$

where the derivative $f'(b/R)$ is given by

$$f'\left(\frac{b}{R}\right) = \frac{2}{\alpha^2}\left\{\left[2(2-\alpha)\left(\frac{b}{R}\right)^{1-\alpha} + 2(\alpha+1)\left(\frac{b}{R}\right)^{2\alpha+1} - 6\left(\frac{b}{R}\right)\right] + \frac{\mathrm{d}}{\mathrm{d}(b/R)}\int_1^\infty g\left(\frac{b}{R},\eta\right)\mathrm{d}\eta\right\}. \tag{3.19}$$

Note that this value of b/R depends only upon the non-dimensional groups $J_{IIC}/\mu R$ and α. Consequently, the minimum value $p_{F\,min}/\mu$ is a function of $J_{IIC}/\mu R$ and

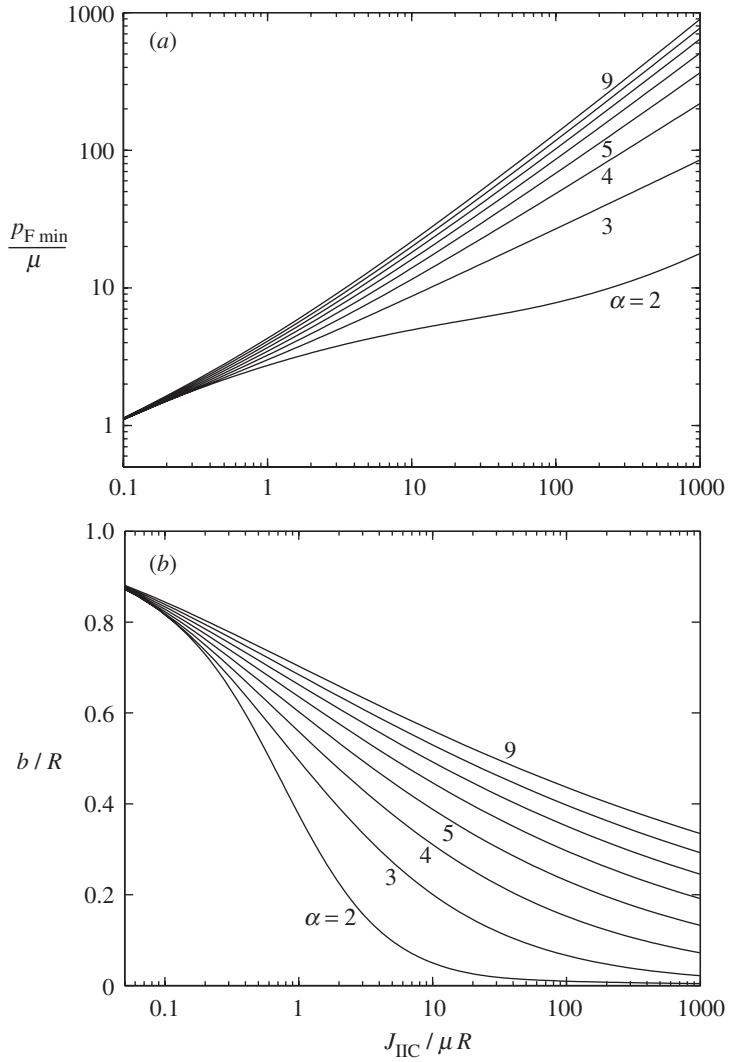

Figure 5. Prediction of (*a*) $p_{\mathrm{F\,min}}/\mu$ versus $J_{\mathrm{IIC}}/\mu R$ and (*b*) b/R versus $J_{\mathrm{IIC}}/\mu R$ for the penetration of a soft solid by a flat-bottomed punch.

α. For any assumed value of $J_{\mathrm{IIC}}/\mu R$ and α, the relations (3.18) and (3.19) can be evaluated by numerical integration of (3.12) in order to obtain the value of b/R which minimize p_{F}/μ. The minimum pressure $p_{\mathrm{F\,min}}/\mu$ is then determined from (3.5) and (3.17). The predicted dependence of $p_{\mathrm{F\,min}}/\mu$ upon $J_{\mathrm{IIC}}/\mu R$, with corresponding values of b/R, is shown in figure 5, for selected values of α. It is clear from the figure that $p_{\mathrm{F\,min}}/\mu$ increases and b/R decreases with increasing $J_{\mathrm{IIC}}/\mu R$: an increase in crack-tip toughness leads to a diminished diameter of cylindrical tear, and to an increased penetration pressure, through an increase in stored strain energy within the compressed column and within the solid external to the expanded hole. In contrast, an elevation in strain-hardening index α leads to an increased pressure $p_{\mathrm{F\,min}}/\mu$ and a larger associated hole diameter b/R.

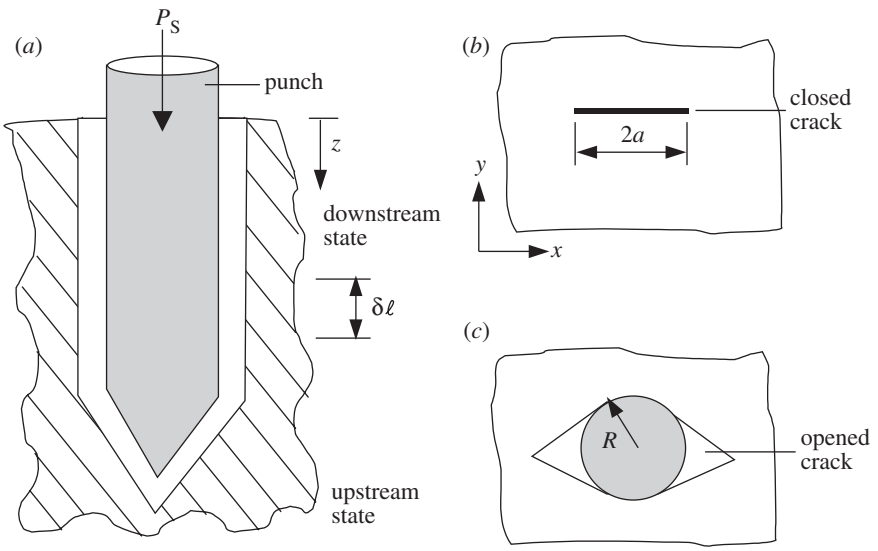

Figure 6. (*a*) Penetration of a soft solid by a sharp-tipped punch. (*b*) Formation of a plane-strain crack of length $2a$ in an infinite slice of thickness $\delta\ell$. (*c*) Opening of the crack by an expanding circular cylinder to a final radius R.

4. Sharp-tipped punch penetration model

We now consider the penetration of a soft solid by a sharp-tipped punch. We calculate the steady-state penetration force to advance and open a crack at the punch tip. The model includes a condition for determining the stable crack length along the flanks of the punch.

Consider a frictionless, rigid cylindrical punch of radius R with a conical tip pushed into a semi-infinite block, as shown in figure 2a. The solid tears and opens at the tip of the punch. The detailed solution for the punch tip requires a full three-dimensional calculation; however, we can consider a punch advance by $\delta\ell$ as equivalent to creating a plane-strain crack of length $2a$ in a slice of thickness $\delta\ell$, and then opening the crack to accommodate the punch. This energy-balance approach is accurate when the strain-energy density in each material element is independent of strain path.

Consider the steady-state advance of the punch by an axial increment $\delta\ell$ due to a load P_S. The work done by the punch in effecting this advance is $P_S\delta\ell$. This work increment balances the energy δW_C required to form a crack of length $2a$ in a solid slice of thickness $\delta\ell$ (see figure 6*b*), and the strain energy stored in the solid δS_E upon opening the crack to accommodate a circular cylindrical inclusion of radius R (see figure 6*c*). Hence,

$$P_S\delta\ell = \delta W_C + \delta S_E. \tag{4.1}$$

The work required to create the crack, δW_C, is determined by the mode-I toughness of the material, J_{IC} and is given by

$$\delta W_C = 2J_{IC}a\delta\ell. \tag{4.2}$$

In order to calculate the work δS_E required to wedge open the crack, we consider the auxiliary problem of expanding a circular wedge of radius R' from $R' = 0$ to a

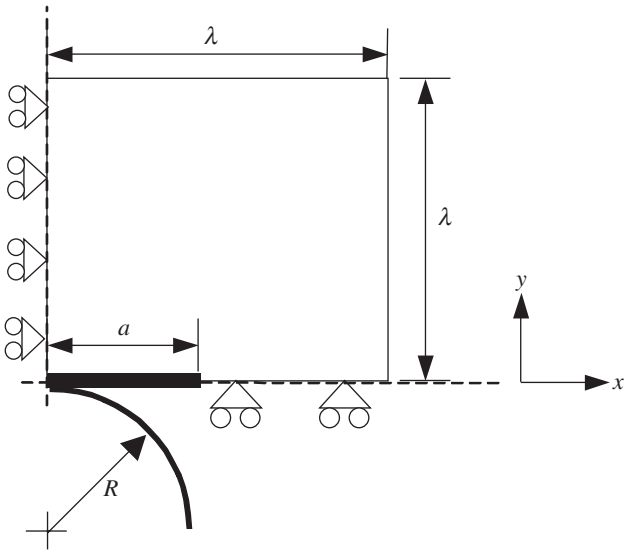

Figure 7. Sketch of the finite-element model for a plane-strain crack wedged open by a circular cylindrical punch. Side length λ is taken to be much greater than the crack length a, at $\lambda = 20a$.

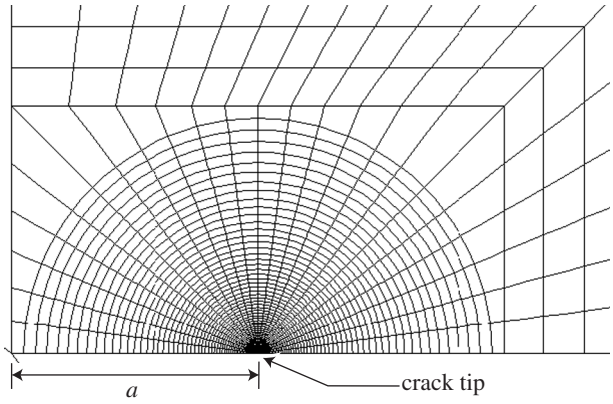

Figure 8. Mesh detail of the radial elements used to model the region around the crack tip.

final value of $R' = R$. It is convenient to write δS_{E} as

$$\delta S_{\mathrm{E}} = \mu R^2 h\left(\frac{a}{R}\right)\delta\ell, \tag{4.3}$$

where the dimensionless function $h(a/R)$ is evaluated explicitly using a finite-element procedure, outlined below.

The sum of (4.2) and (4.3) gives the work done by the punch,

$$P_{\mathrm{S}}\delta\ell = 2J_{\mathrm{IC}}a\delta\ell + \mu R^2 h\left(\frac{a}{R}\right)\delta\ell, \tag{4.4}$$

and the average penetration pressure p_{S} on the punch follows immediately as

$$\frac{p_{\mathrm{S}}}{\mu} = \frac{P_{\mathrm{S}}}{\pi\mu R^2} = \frac{2}{\pi}\left(\frac{J_{\mathrm{IC}}}{\mu R}\right)\left(\frac{a}{R}\right) + \frac{1}{\pi}h\left(\frac{a}{R}\right). \tag{4.5}$$

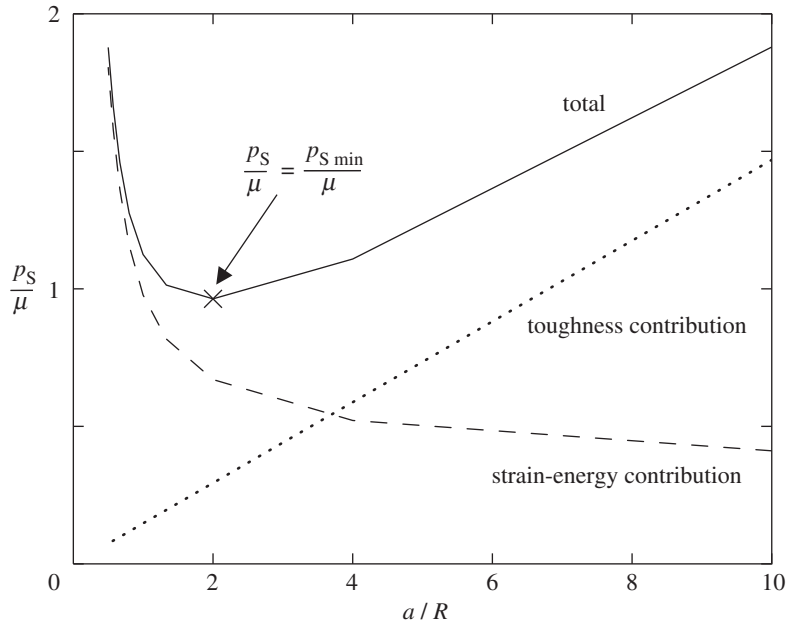

Figure 9. Contributions to p_S/μ from crack toughness and strain energy due to crack opening ($\alpha = 3$, $J_{IC}/\mu R = 0.23$).

(*a*) *A finite-element approach to evaluate* $h(a/R)$

A finite-element approach is used to determine $h(a/R)$ for selected values of α. The finite-element model is shown in figure 7. Considerations of symmetry allow us to model only a quadrant of the crack and punch. The initial configuration is taken to be a closed crack of length $2a$ within a square block of side length 2λ, where λ is taken to be much greater than the crack length ($\lambda = 20a$). A rigid frictionless punch of radius R is in point contact with the midpoint of the crack. Plane strain, eight-noded, quadrilateral elements are used to mesh the hyperelastic solid block. The region around the crack tip is meshed using a radial configuration of elements centred at the crack tip, as shown in figure 8. Triangular elements are required for the innermost circumference of elements at the crack tip. These triangular elements are formed by collapsing one side of a four-sided element to a point, in order to handle the crack singularity (Tracey 1976). The remainder of the block is meshed using a rectangular grid of elements. Appropriate roller-boundary conditions are prescribed on symmetry planes as sketched in figure 7, with the crack flanks traction-free where not in contact with the frictionless punch. The punch is displaced in incremental steps up to an indentation depth of magnitude R. The stored strain energy in the solid and the plane-strain energy release rate at the crack tip are determined in the final state.

(*b*) *Prediction of the crack length in steady-state penetration*

The finite-element predictions for p_S/μ versus a/R are shown in figure 9, for the choice $\alpha = 3$. Also shown are the separate contributions to p_S/μ from the fracture work and the stored strain energy associated with crack opening. For low values of

a/R the strain energy associated with crack opening is the dominant contributor to p_{S}/μ, while at high values of a/R the work of crack formation is the dominant contributor. The pressure attains a global minimum value $p_{\mathrm{S\,min}}/\mu$ at an intermediate value of a/R.

It is argued that stable penetration occurs when p_{S}/μ achieves this minimum value of pressure. Differentiation of relation (4.5) with respect to a/R gives

$$2\frac{J_{\mathrm{IC}}}{\mu R} + h'\left(\frac{a}{R}\right) = 0. \tag{4.6}$$

This expression is used to obtain the crack length during steady-state penetration.

At the tip of the open crack along the flanks, the plane-strain energy release rate J_{PS} for crack advance in a slice of thickness $\delta\ell$ is

$$J_{\mathrm{PS}} = -\frac{1}{2\delta\ell}\frac{\partial S_{\mathrm{E}}}{\partial a} = -\tfrac{1}{2}\mu R h'\left(\frac{a}{R}\right). \tag{4.7}$$

Substitution of (4.6) into (4.7) reveals that the energy release rate for the crack along the flanks of the advancing punch is at incipient crack advance:

$$J_{\mathrm{PS}} = J_{\mathrm{IC}}. \tag{4.8}$$

Additionally, the incipient crack advance along the flanks of the punch is stable: the slope of the J_{PS} versus crack length a is negative,

$$\frac{\partial J_{\mathrm{PS}}}{\partial a} < 0. \tag{4.9}$$

at fixed R.

(*c*) *Results of the finite-element analysis*

The dependence of $p_{\mathrm{S\,min}}/\mu$, and the corresponding value of a/R, upon $J_{\mathrm{IC}}/\mu R$ and α has been evaluated using the above finite-element method. The results of this analysis are shown in figure 10. As for the case of the flat-bottomed punch, $p_{\mathrm{S\,min}}/\mu$ increases while a/R decreases with increasing $J_{\mathrm{IC}}/\mu R$. An increase in strain-hardening exponent α leads to an increase in both $p_{\mathrm{S\,min}}/\mu$ and a/R.

5. Comparison of the model predictions with measured penetration pressures

A comparison of the predicted penetration pressures $p_{\mathrm{F\,min}}/\mu$ and $p_{\mathrm{S\,min}}/\mu$ versus $J_{\mathrm{C}}/\mu R$ is plotted in figure 11. For both punch geometries p/μ increases with increasing $J_{\mathrm{C}}/\mu R$ and strain-hardening exponent α, as expected. The penetration pressure for a flat-bottomed punch $p_{\mathrm{F\,min}}/\mu$ is two to three times greater than that for a sharp-tipped punch, $p_{\mathrm{S\,min}}/\mu$, assuming that J_{IIC} is taken to equal J_{IC} (reasonable for a rubber-like material).

(*a*) *Sharp-tipped punch*

The predictions of the penetration model for a sharp-tipped punch are now compared with measured penetration pressures, as reported by Shergold & Fleck (2004)

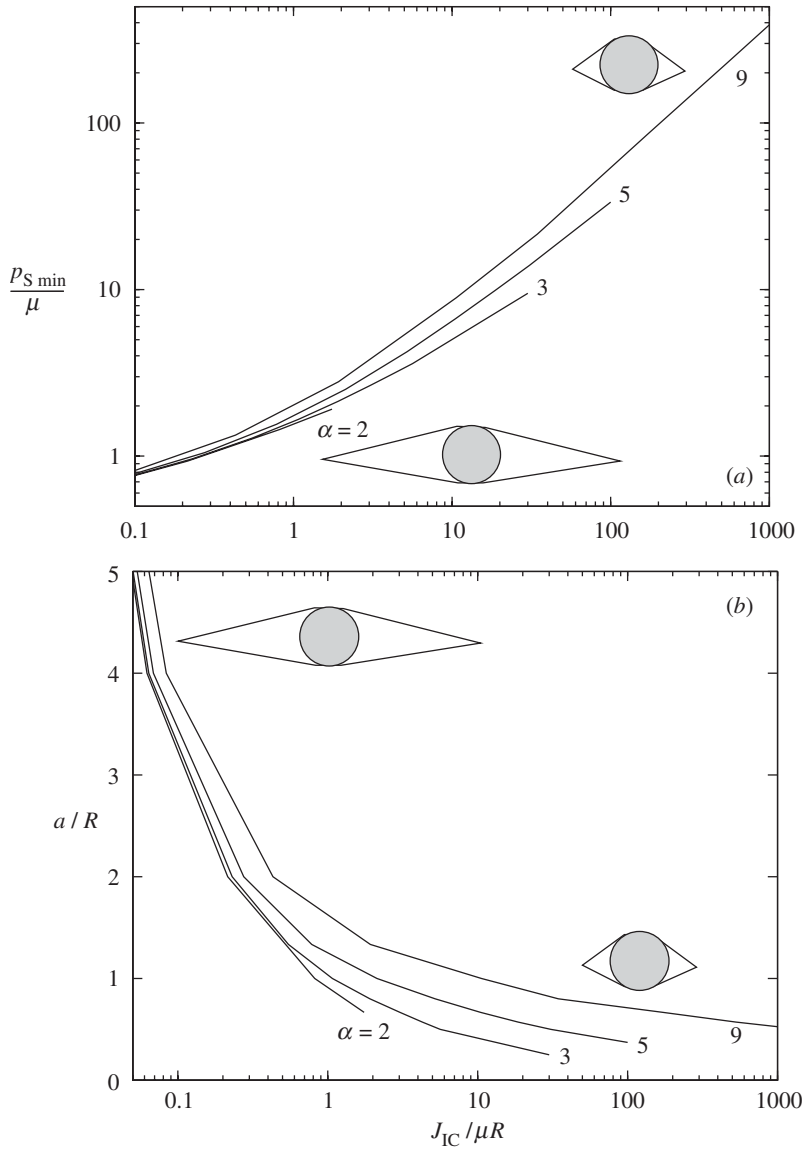

Figure 10. Prediction of (*a*) $p_{S\,min}/\mu$ versus $J_{IC}/\mu R$, and (*b*) a/R versus $J_{IC}/\mu R$, for the penetration of a soft solid by a sharp punch.

and by Frick *et al*. (2001). Shergold & Fleck (2004) used hypodermic needles to penetrate human skin *in vivo*, and conically tipped punches to penetrate two grades of silicone rubber (B452 and Sil8800), while Frick *et al*. (2001) performed penetration experiments on sheepskin *in vitro* using suture needles. Here, we assume that the stress-versus-strain response and toughness of sheep skin are adequately represented by the measured data for human skin.

In order to compare the model with measured data, it is important to use the most appropriate values of measured toughness. An examination of the literature suggests that the measured toughness of skin is sensitive to the type of toughness

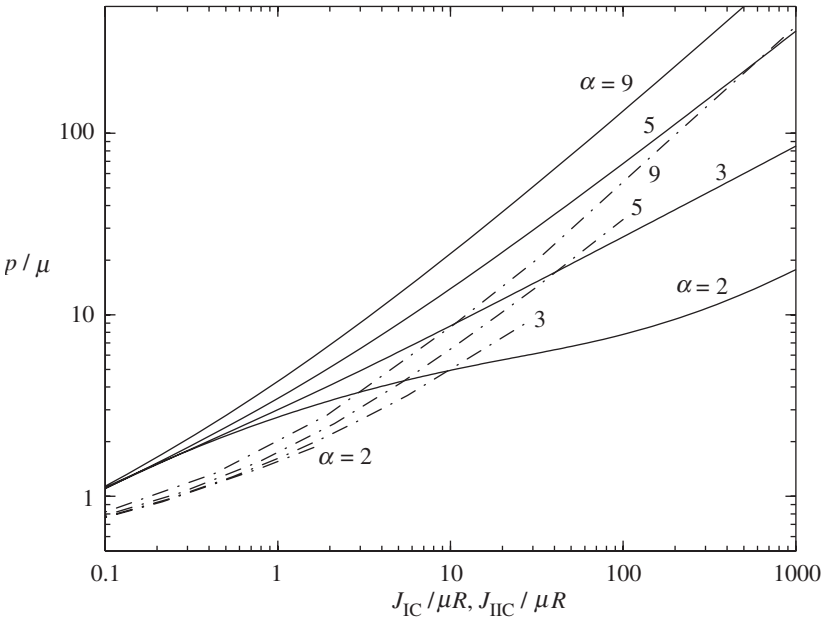

Figure 11. Comparison of p/μ versus $J/\mu R$ for penetration of a solid by a flat-bottomed punch (———, $p_{\mathrm{F\,min}}/\mu$) and a sharp-tipped punch (— · — · —, $p_{\mathrm{S\,min}}/\mu$).

Table 3. *Sharp-tipped penetrators used in penetration experiments on silicone rubber, human skin in vivo (Shergold & Fleck 2004) and sheep skin in vitro (Frick et al. 2001)*

solid	grade	type of penetrator	diameter of penetrator (mm)
silicone rubber	Sil8800	conical-tipped punch	0.5, 1.0, 2.0
silicone rubber	B452	conical-tipped punch	1.0, 2.0
skin	human	hypodermic needle	0.3, 0.6
skin	sheep	suture needle	1.0

test performed. Scissor tear tests maintain a sharp crack tip and give a low toughness value of $2.5\,\mathrm{kJ\,m^{-2}}$ for human skin. It is argued that the chamfered edges of a hypodermic needle and of a suture needle also maintain a sharp crack tip and thereby induce a low toughness value (see, for example, Lake & Yeoh 1978, 1987). In contrast, the trouser-tear test allows the crack tip to blunt in a toughness test and thereby gives rise to a larger measured toughness. This is consistent with the fact that the toughness of rat skin measured by a trouser-tear test (Purslow 1983) is an order of magnitude higher than the toughness measured by a scissor tear test (Pereira *et al.* 1997). It is argued that the degree of crack blunting during the penetration of the silicone rubbers by a conically tipped punch is similar to that observed in a trouser-tear test. Consequently, measured trouser-tear values of toughness are used for the silicone rubbers.

Figure 12*a* shows the predicted response of $p_{\mathrm{S\,min}}/\mu$ versus $J_{\mathrm{IC}}/\mu R$ for the sharp-tipped punch penetration model, while the relation between a/R and $J_{\mathrm{IC}}/\mu R$ is given in figure 12*b*. The results of the penetration experiments are included. In the exper-

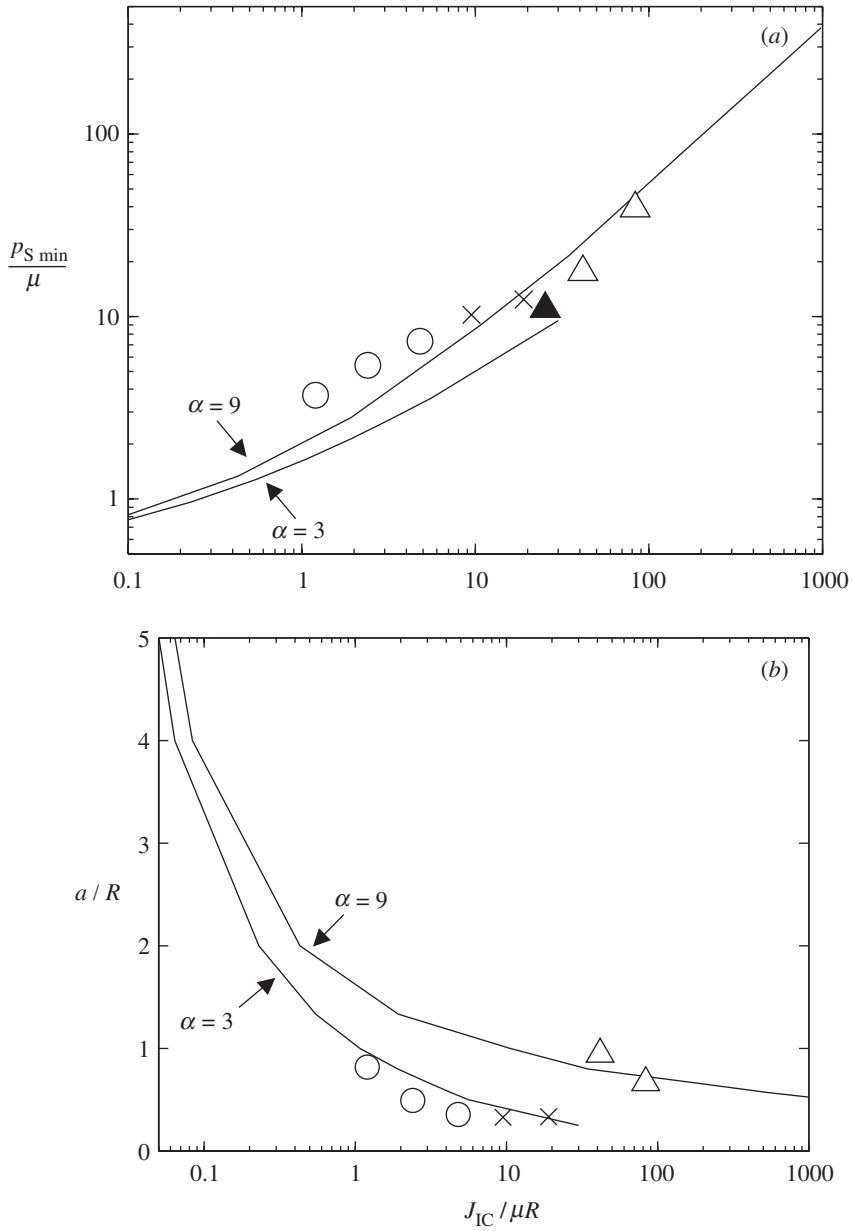

Figure 12. (*a*) $p_{S\,min}/\mu$ versus $J_{IC}/\mu R$ and (*b*) a/R versus $J_{IC}/\mu R$ for the penetration of a soft solid by a sharp-tipped punch. ∘, Sil8800 ($\alpha = 2.5$, $J_{IC} = 3.1\,\mathrm{kJ\,m^{-2}}$); ×, B452 ($\alpha = 3.0$, $J_{IC} = 3.8\,\mathrm{kJ\,m^{-2}}$); △, human skin ($\alpha = 9.0$, $J_{IC} = 2.5\,\mathrm{kJ\,m^{-2}}$); ▲, sheep skin ($\alpha = 9.0$, $J_{IC} = 2.5\,\mathrm{kJ\,m^{-2}}$).

imental investigations the independent parameter $J_{IC}/\mu R$ was varied by selecting a range of values of punch radius R, as given in table 3.

The experiments validate the predictions of the sharp-tipped penetration model across a wide range of values for $J_{IC}/\mu R$ and α. There is good agreement between

the predicted and measured crack lengths for human skin and silicone rubber. The predicted penetration pressures for human skin and sheep skin are also reasonably accurate. However, the predicted penetration pressures of the silicone rubbers are less accurate, with the predicted value being about half the measured value. The reasons for this are unclear, but may reflect the sensitivity of the measurements to the mechanical properties. In broad terms however, the predicted trends reflect those measured.

(*b*) *Flat-bottomed punch*

The flat-bottomed punch penetration model is compared with the experiments of Shergold & Fleck (2004) on silicone rubbers (B452 and Sil8800) and human skin in figure 13. Shergold & Fleck (2004) used a 0.3 mm diameter punch to penetrate human skin *in vivo* and a 1.0 mm diameter punch to penetrate the silicone rubbers. It is argued that penetration by a flat-bottomed punch gives rise to a similar degree of crack-tip blunting to that achieved in a trouser-tear test. Consequently, the toughness values from trouser-tear tests are used to compare the penetration experiments with the model predictions. Unfortunately this toughness value is not available for human skin, and so the measured trouser-tear test value for rat skin (Purslow 1983) is used instead.

Figure 13*a* shows the comparison of the flat-bottomed punch model and the experiments for $p_{\mathrm{F\,min}}/\mu$ versus $J_{\mathrm{IIC}}/\mu R$ and figure 13*b* shows that for b/R versus $J_{\mathrm{IIC}}/\mu R$. The predicted penetration pressures are adequate for the rubbers and skin. Although the predicted hole diameter is reasonably accurate for the rubbers, the predicted value for skin is about half the measured value. A possible explanation lies in the fact that the measured hole diameter for the skin is limited to a surface measurement, as the experiments were performed *in vivo*. The experiments on rubber reveal that the hole diameter at the surface is about twice the value at depth; in rubber penetration, the values at depth were easily measured by sectioning *a posteriori*, and these steady-state values are shown in the plot. It was not practical to measure the steady-state value of the hole diameter of the skin.

6. Concluding remarks

Penetration models have been developed for the pressure required to penetrate a soft solid by either a sharp-tipped or a flat-bottomed punch. The models have been validated by a comparison of the predictions with the measured steady-state pressure for two silicone rubbers, and for human skin and sheep skin. It is predicted that the penetration pressure for both sharp-tipped and flat-bottomed punches increases with the non-dimensional group of $J_{\mathrm{C}}/\mu R$ and with the strain-hardening exponent α. Previous penetration models, based upon the expansion of a spherical or cylindrical cavity, without cracking, predict penetration pressures that greatly exceed the measured values.

The use of a sharpened hypodermic needle to administer an injection is a long established medical technique. The current study reveals that such an injection leads to the formation of a crack rather than to a residual hole in the dermis. This has the advantage that the wound can self-seal.

We have assumed in our analysis that skin is transversely isotropic. In reality, the dermis is more accurately represented by an orthotropic elastic solid. The above

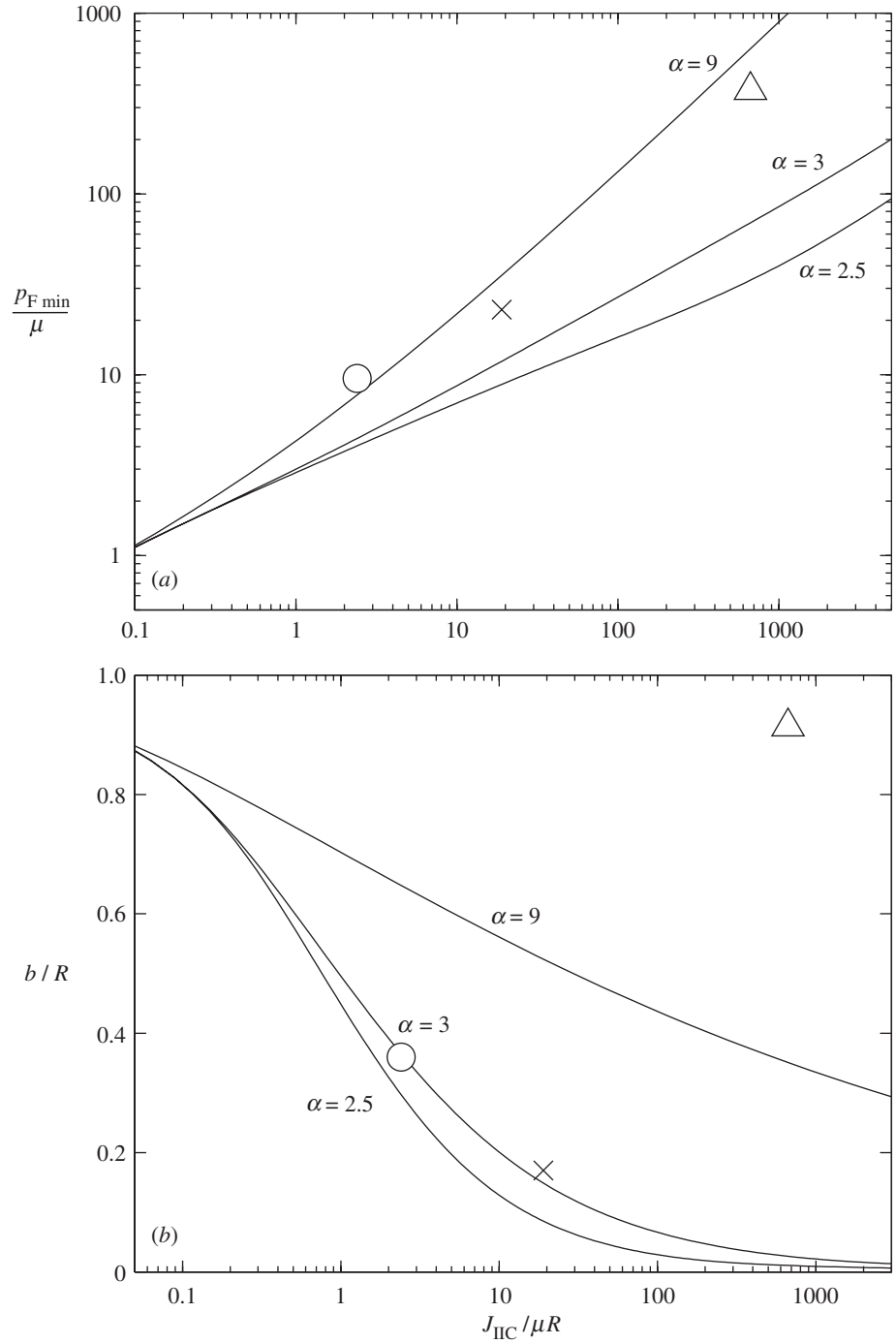

Figure 13. (*a*) $p_{\mathrm{F\,min}}/\mu$ versus $J_{\mathrm{IIC}}/\mu R$ and (*b*) p/μ versus $J_{\mathrm{IIC}}/\mu R$ for penetration of a soft solid by a flat-bottomed punch. ∘, Sil8000 ($\alpha = 2.5$, $J_{\mathrm{IIC}} = 3.1\ \mathrm{kJ\ m^{-2}}$); ×, B452 ($\alpha = 3.0$, $J_{\mathrm{IIC}} = 3.8\ \mathrm{kJ\ m^{-2}}$); △, human skin ($\alpha = 9.0$, $J_{\mathrm{IIC}} = 20\ \mathrm{kJ\ m^{-2}}$).

models can be extended to the orthotropic case, and this warrants future investigation.

This research was funded by grants from Weston Medical, the Engineering and Physical Sciences Research Council and the Royal Commission for the Exhibition of 1851.

References

Ankerson, J., Birkbeck, A. E., Thomson, R. D. & Vanezis, P. 1998 The effect of knife blade profile on penetration force in flesh simulants. *Tech. Law Insurance* **3**, 125–128.

Ankerson, J., Birkbeck, A. E., Thomson, R. D. & Vanezis, P. 1999 Puncture resistance and tensile strength of skin simulants. *Proc. Instn Mech. Engrs* H **213**, 493–501.

Bishop, R. F., Hill, R. & Mott, N. F. 1945 The theory of indentation and hardness tests. *Proc. Phys. Soc.* **57**, 147–159.

Black, D., Marks, R. & Caunt, A. 1985 Measurement of scalpel blade sharpness and its relationship to wound healing. *Bioengng Skin* **1**, 111–123.

Brett, P. N., Parker, T. J., Harrison, A. J., Thomas, T. A. & Carr, A. 1997 Simulation of resistance forces acting on surgical needles. *Proc. Instn Mech. Engrs* H **211**, 335–347.

Charrier, J. M., Maki, S. G., Chalifoux, J. P. & Gent, A. N. 1986 Penetration of elastomeric blocks by needles. *J. Elastom. Plast.* **18**, 200–210.

Cooper, J. A., Bromley, L. M., Baranowski, A. & Barker, S. G. E. 2000 Evaluation of a needle-free injection system for local anaesthesia prior to venous cannulation. *Anaesthesia* **55**, 247–250.

Figge, F. H. J. & Barnet, D. J. 1948 Anatomic evaluation of a jet injection instrument designed to minimize pain and inconvenience of parenteral therapy. *Am. Practition.* **3**, 197–206.

Frick, T. B., Marucci, D. D., Cartmill, J. A., Martin, C. J. & Walsh, W. R. 2001 Resistance force acting on suture needles. *J. Biomech.* **34**, 1335–1340.

Fung, Y. C. 1981 *Biomechanics: mechanical properties of living tissues*. Springer.

Gibson, R. E. 1950 Correspondence on the bearing capacity of screw piles and screwcrete cylinders. *J. Instn Civil Engrs* **34**, 382–383.

Gibson, R. E. & Anderson, W. F. 1961 *In situ* measurement of soil properties with the pressuremeter. *Civ. Engng Publ. Works Rev.* **56**, 615–618.

Hill, R. 1950 *The mathematical theory of plasticity*. Oxford University Press.

Jansen, L. H. & Rottier, P. B. 1958 Some mechanical properties of human abdominal skin measured on excised strips: a study of their dependence on age and how they are influenced by the presence of striae. *Dermatologica* **117**, 65–183.

Katakura, H. & Tsuji, S. 1985 A study to avoid the dangers of high speed liquid jets. *Bull. Jpn Soc. Mech. Engng* **28**, 623–630.

Knight, B. 1975 The dynamics of stab wounds. *Forensic Sci.* **6**, 249–255.

Lake, G. J. & Yeoh, O. H. 1978 Measurement of rubber cutting resistance in the absence of friction. *Int. J. Fracture* **14**, 509–526.

Lake, G. J. & Yeoh, O. H. 1987 Effect of crack tip sharpness on the strength of vulcanized rubbers. *J. Polym. Sci.* B **25**, 1157–1190.

Livingston, D. I., Yeh, G. S., Rohall, P. & Gehman, S. D. 1961 Visco-elastic factors in the strength of elastomers under complex stress by a puncture method. *J. Appl. Polym. Sci.* **5**, 442–451.

Maas, A. J. & Brink, P. R. G. 1987 Some physical aspects of the medical jet injector. *Med. Biol. Engng Comput.* **25**, 81–86.

North, J. & Gibson, F. 1978 Volume compressibility of human abdominal skin. *J. Biomech.* **11**, 203–207.

O'Callaghan, P. T., Jones, M. D., James, D. S., Leadbeatter, S., Holt, C. A. & Nokes, L. D. M. 1999 Dynamics of stab wounds: force required for penetration of various cadaveric human tissues. *Forensic Sci. Int.* **104**, 173–178.

Ogden, R. W. 1972 Large deformation isotropic elasticity: on the correlation of theory and experiment for incompressible rubberlike solids. *Proc. R. Soc. Lond.* A **326**, 565–584.

Pereira, B. P., Lucas, P. W. & Swee-Hin, T. 1997 Ranking the fracture toughness of thin mammalian soft tissues using the scissors cutting test. *J. Biomech.* **30**, 91–94.

Purslow, P. 1983 Measurement of the fracture toughness of extensible connective tissues. *J. Mater. Sci.* **18**, 3591–3598.

Reihsner, R., Balogh, B. & Menzel, E. J. 1995 Two-dimensional elastic properties of human skin in terms of an incremental model at the *in vivo* configuration. *Med. Engng Phys.* **17**, 304–313.

Schramm, J. & Mitragotri, S. 2002 Transdermal drug delivery by jet injectors: energetics of jet formation and penetration. *Pharmaceut. Res.* **19**, 1673–1679.

Scott, C. R. 1980 *An introduction to soil mechanics and foundations*. London: Applied Science Publishers.

Shergold, O. A. & Fleck, N. A. 2004 Experimental investigation into the penetration of soft solids. (Submitted.)

Stephens, R. R. & Kramer, I. R. H. 1964 Intra-oral injections by high pressure jet. *Br. Dent. J.* **117**, 465–476.

Stevenson, A. & Abmalek, K. 1994 On the puncture mechanics of rubber. *Rubber Chem. Technol.* **67**, 743–760.

Towler, M. A., McGregor, W., Rodeheaver, G. T., Cutler, P. V., Bond, R. F., Phung, D., Morgan, R. G., Thacker, J. G. & Edlich, R. F. 1988 Influence of cutting edge configuration on surgical needle penetration forces. *J. Emerg. Med.* **6**, 475–481.

Tracey, D. M. 1976 Finite element solutions for crack-tip behavior in small-scale yielding. *J. Engng Mater. Technol.* **98**(2), 146–151.

Verhagen, A., Ebels, J. T., Dogterom, A. A. & Jonkman, J. H. G. 1995 Pharmacokinetics and pharmacodynamics of a single dose of recombinant human growth hormone after subcutaneous adminstration by jet-injection: comparison with conventional needle-injection. *Eur. J. Clin. Pharmacol.* **49**, 69–72.

Vijay, M. M. 1989 A critical examination of the use of water jets for medical applications. In *Proc. 5th American Water Jet Conf., Toronto, Canada*, pp. 425–448. Ottawa: National Research Council of Canada.

Vossoughi, J. & Vaishnav, R. 1979 Comments on the paper 'Volume compressibility of human abdominal skin'. *J. Biomech.* **12**, 481.

Wright, S. C., Huang, Y. & Fleck, N. A. 1992 Deep penetration of polycarbonate by a cylindrical punch. *Mech. Mater.* **13**, 277–284.